Environmental Science & Technology

Article

pubs.acs.org/est

Interfacial Tensions of Aged Organic Aerosol Particle Mimics Using a Biphasic Microfluidic Platform

Andrew R. Metcalf, Hallie C. Boyer, and Cari S. Dutcher*

Department of Mechanical Engineering, University of Minnesota, Twin Cities, Minneapolis, Minnesota, 55455 United States

ABSTRACT: Secondary organic aerosol (SOA) particles are a major component of atmospheric particulate matter, yet their formation processes and ambient properties are not well understood. These complex particles often contain multiple interfaces due to internal aqueous- and organic-phase partitioning. Aerosol interfaces can profoundly affect the fate of condensable organic compounds emitted into the atmosphere by altering the way in which ambient organic vapors interact with suspended particles. To accurately predict the evolution of SOA in the atmosphere, we must improve our understanding of aerosol interfaces. In this work, biphasic microscale flows are used to measure interfacial tension of reacting methylglyoxal, formaldehyde, and ammonium sulfate aqueous mixtures with a surrounding oil phase. Our experiments show a suppression of interfacial tension as a function of organic content that remains constant with reaction time for methylglyoxal—ammonium sulfate systems. We also reveal an unexpected time dependence of interfacial tension over a period of 48 h for ternary solutions of both methylglyoxal and formaldehyde in aqueous ammonium sulfate, indicating a more complicated behavior of surface activity where there is competition among dissolved organics. From these interfacial tension measurements, the morphology of aged atmospheric aerosols with internal liquid−liquid phase separation is inferred.

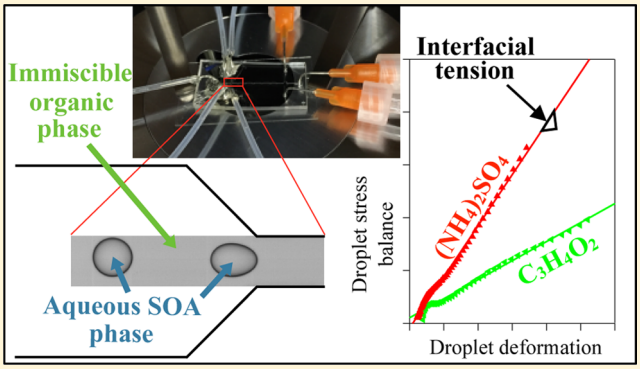

INTRODUCTION

Secondary organic aerosol (SOA) particles are nearly ubiquitous in the atmosphere,[1−3] and yet there remains large uncertainties in their formation processes and ambient properties.[4,5] These particles are complex microenvironments that can contain multiple interfaces due to internal liquid−liquid phase separation and to the external liquid−vapor surface. These aerosol interfaces can profoundly affect the fate of condensable organic compounds emitted into the atmosphere by altering the way in which organic vapors interact with the ambient aerosol. For example, organic thin films can shield the core of the aerosol from the ambient environment, which may disrupt equilibrium partitioning and mass transfer. To further understand SOA behavior in the atmosphere, it is necessary to investigate aerosol interfaces arising from liquid−liquid phase separation within aqueous aerosol.[6]

The presence of surface active constituents (i.e., organic acids, diacids, proteins, and humiclike substances) in atmospheric aerosol leads to the formation of surface films on aerosol particles due to hydrophobic groups preferentially protruding out of the particle into the surrounding gas phase.[7] Surface-active organics are known to reduce surface tension,[8,9] inhibit gas-phase uptake into[10−12] and evaporation from[13−15] the bulk of the aerosol, enhance ice[16] and cloud[17,18] condensation nucleation, and modify heterogeneous chemistry[19,20] and optical properties.[21] Some studies have shown that organic coatings actually do not have much effect on particles' ability to deliquesce or effloresce[22−24] or act as ice nuclei,[25] suggesting that particle morphology (i.e., incomplete coating of the organic) plays an important role in determining how particles behave in the atmosphere. However, the exact microphysical structure of ambient aerosol remains highly uncertain and under-investigated.[4] Traditionally, ambient aerosol containing multiple condensed species has been modeled as well-mixed, homogeneous liquid droplets using volume- or mass-mixing rules for the different species (e.g., ref 26). Many recent studies, though, have observed liquid−liquid phase separation in aerosol mimics in the laboratory,[27−29] leading to the identification of other aerosol morphologies, including thin-film (core−shell) structures,[14,18,30−33] partially engulfed lenses,[34−36] micelle-like aggregates,[37] solid inclusions,[38] liquid−liquid phase-separated islands (e.g., from spinodal decomposition),[39,40] and other multiphase-separated structures.[41,42] Predictions of ambient aerosol morphology are further complicated by the dependence of particle-phase chemical composition on environmental factors such as temperature and relative humidity.

Recently, a thermodynamic model of equilibrium morphology for an immiscible three-phase system of liquid drops in air based on spreading coefficients[43−45] was applied to mixed inorganic−organic aerosol.[29,33,34] The model assumes that the

Received: October 5, 2015
Revised: December 21, 2015
Accepted: December 29, 2015
Published: December 29, 2015

DOI: 10.1021/acs.est.5b04880
Environ. Sci. Technol. 2016, 50, 1251−1259

equilibrium configuration of a compound particle will have the lowest-total surface free energy

$$G_s = \sum \gamma_{ij} A_{ij} \quad (1)$$

where γ_{ij} is the interfacial tension (IFT) between phases i and j, and A_{ij} is the interfacial area between those respective phases. The spreading coefficient, S_i, is defined by

$$S_i = -\Delta G_s / A \quad (2)$$

where ΔG_s is the free-energy increase due to spreading of liquid i over another substrate (solid or liquid).[46] Thus, the spreading coefficient is the difference in surface energy between a dry substrate, in which no spreading takes place, and that of a wet substrate over which liquid i has spread. If S_i is positive, then spreading takes place spontaneously and evenly over the substrate; otherwise, the liquid will form a partial droplet, or surface lens, on the substrate.[46,47] Rewriting the spreading coefficient in terms of interfacial tension, eq 2 becomes

$$S_i = \gamma_{jk} - (\gamma_{ij} + \gamma_{ik}) \quad (3)$$

For phase-separated aerosol particles in air, the three-phase system is designated by the aqueous, organic, and gas phases labeled 1, 2, and 3, respectively. Thus, S_1 is the spreading of the aqueous phase over the organic phase and, due to interfacial tensions relevant to atmospheric aerosol, is assumed to always be negative, or to cost energy, and will not occur naturally in the atmosphere.[34] The spreading coefficient of the organic phase (S_2) and of air (S_3) can be positive or negative. Therefore, the possible particle configurations for an aerosol consisting of immiscible aqueous and organic phases are *nonengulfing* ($S_2 < 0$, $S_3 > 0$), where the two phases exist as side-by-side droplets with minimal contact; *complete engulfing* ($S_2 > 0$, $S_3 < 0$), where the organic phase completely surrounds the aqueous phase; and *partially engulfing* (S_2, $S_3 < 0$), the exact nature of which then depends on the volumes of each phase present in the whole particle.[29,34,35] By calculating the spreading coefficients for the relevant species in an aerosol particle, one can determine if the aerosol morphology is core–shell (i.e., completely engulfing) or partially engulfing. This spreading coefficient framework for predicting aerosol morphology has been validated for aerosols larger than ∼100 nm in diameter by comparison with molecular dynamics simulations[48] and experimental data.[29] Thus, knowledge of the interfacial tensions among the chemical constituents relevant for ambient aerosol is important for predicting the morphology of liquid–liquid phase-separated aerosol.

One important constituent in ambient aerosol is methylglyoxal (MG, $C_3H_4O_2$), an oxidation product of many biogenic[49] and anthropogenic[50−54] volatile organic compounds (VOCs) and found in the gas phase at ppbv mixing ratios in urban atmospheres.[55−57] MG also partitions to the aqueous phase where it enhances cloud condensation nuclei (CCN) activity[58] and can be hydrated to form oligomers in solution.[59−61] MG has been detected in rain and cloud drops[62] and, with subsequent oligomerization, could result in organic material that remains in the particle phase after the evaporation of liquid droplets.[63]

Sareen et al. (2010)[64] studied the aqueous reactions of MG with ammonium salts and found that with reaction time (a proxy for aging of atmospheric aerosol), light-absorbing secondary products form in solution that additionally suppress the bulk surface tension of the mixture. The surface activity of species in these solutions is attributed to a methyl group, which adds hydrophobicity to MG and its oligomer products.[64] A detailed study[65] combining theory and measurements reveals that in a MG–water system, it is the singly hydrated methylglyoxal diol that populates the surface and is responsible for the surface-tension depression relative to pure water samples. The same singly hydrated MG was observed in a MG–ammonium sulfate (AS) system,[64] possibly explaining the surface tension depression observed for those systems as well.

Likewise, formaldehyde (F, CH_2O) is found at ppbv mixing ratios in urban atmospheres[66] and is both emitted directly and formed during atmospheric oxidation of some VOCs.[1,67] Reactions of formaldehyde with amines and carbonyls yield relatively nonvolatile and chemically stable organic salts,[68] which could explain the substantial amount of formaldehyde signal in the aerosol phase.[66] Aqueous formaldehyde can also form oligomers in solution,[67,69,70] similar to MG. Because of these oligomerization pathways, a combined MG–F–AS system was studied.[71,72] It was found that ternary mixtures of MG and either formaldehyde or acetaldehyde with AS exhibited surface tension behavior similar to binary mixtures with only MG with AS, indicating that MG is the dominant driver of surface activity in these solutions, likely due to the presence of the same singly hydrated MG molecule in solution.

The connection between surface-active organics and particle-mixing state has not been well parameterized.[7] In this paper, we present an experimental framework to assess the interfacial activity of dissolved species in MG–F–AS aqueous systems. Specifically, we use biphasic microfluidics to measure the interfacial tension between an aqueous and an oil phase. These microfluidic experiments utilize high-speed imaging to monitor interfacial phenomena at the microscale. From these observations of interfacial tension of aerosol chemical mimics, the behavior and morphology of atmospheric aerosols due to interactions of liquid–liquid phase-separated interfaces within aerosol particles can be inferred.

MATERIALS AND METHODS

To measure interfacial tension, we fabricated a microfluidic device following the design of Hudson et al. (2005).[73] In the microfluidic device, a steady flow of immiscible drops ("dispersed phase") in a carrier fluid ("continuous phase") travels through a series of channel contractions and expansions. Each device is fabricated with multiple contractions and expansions to determine any dependence on interface age. The channel geometry sets up extensional flow fields surrounding the droplets as they enter and exit narrow regions of the device. The droplets deform from an unperturbed, spherical shape to an elongated spheroidal shape due to the extensional stress on the droplet. Hydrodynamic forces are balanced by the interfacial tension at the boundary between the droplet and the surrounding carrier fluid.

The behavior of drop deformation in an extensional flow field is well-established,[74−76] and these results apply to the microscale.[77] The deformation, $D(x)$, is a scalar quantity describing the shape of the droplet as a function of spatial location, x, and is given by

$$D(x) = \frac{r_{major}(x) - r_{minor}(x)}{r_{major}(x) + r_{minor}(x)} \quad (4)$$

where x is the streamwise direction, $r_{major}(x)$ is the major principal radius, and $r_{minor}(x)$ is the minor principal radius of

DOI: 10.1021/acs.est.5b04880
Environ. Sci. Technol. 2016, 50, 1251−1259

the droplet. The principal radii and deformation are functions of the x direction because the droplets experience a changing extensional flow field as they travel through the device. For a Newtonian fluid, the material change of deformation of a spheroidal drop in steady, 1-D flow in the x direction is given by[73,77]

$$u(x)\frac{\partial D(x)}{\partial x} = \frac{5}{2\hat{\eta} + 3}\dot{\varepsilon}(x) - \gamma\frac{\mathrm{D}(x)}{\alpha\eta_c a_0} \tag{5}$$

where, $u(x)$ is droplet velocity, $\hat{\eta} = \eta_d/\eta_c$ is the relative viscosity between the drop (η_d) and surrounding fluid (η_c), $\dot{\varepsilon}(x) = \frac{\partial u(x)}{\partial x}$ is the surrounding fluid extension rate, γ is the interfacial tension, a_0 is the droplet equilibrium radius in the low-shear region of the device, and α is a coefficient

$$\alpha = \frac{(2\hat{\eta} + 3)(19\hat{\eta} + 16)}{40(\hat{\eta} + 1)} \tag{6}$$

which is a function of the relative viscosity. Rearranging eq 5 yields

$$\alpha\eta_c\left(\frac{5}{2\hat{\eta} + 3}\dot{\varepsilon}(x) - u(x)\frac{\partial D(x)}{\partial x}\right) = \gamma\left(\frac{D(x)}{a_0}\right) \tag{7}$$

where every term is known (α, η_c, $\hat{\eta}$) or measured directly from video-microscopy image analysis ($u(x)$, $\dot{\varepsilon}(x)$, $D(x)$, $\partial D(x)/\partial x$, a_0), except interfacial tension, γ.

Droplet deformation is examined in the first contraction region, about 0.15 s after droplet formation, where the device geometry transitions from a wide (750 μm) to narrow (150 μm) channel width. For this study, we report measurements from the first contraction only, as we did not find any dependence on interface age between ~0.15 and ~0.71 s for the systems studied. These steady-state measurements imply that any depletion effects[78] that may be occurring inside each droplet are not affecting the equilibration time of the droplet interface in our system. Further effects of depletion on the absolute value of interfacial tension are not considered here, but it should be noted that similar effects are also expected in atmospheric aerosol of similar chemical composition to the mimic systems studied here.

Upstream of the deformation region, droplets are generated with a T-junction[79] or co-flow[80] geometry, both of which produce monodisperse droplets ~40—150 μm in diameter at a rapid, steady rate. Each droplet is essentially a single-particle experiment that is rapidly repeated with each new droplet formed. In the current configuration, the droplet sizes are larger than the 2—20 μm diameter particles used in other single-particle techniques and are well above typical Kelvin diameters (<~100 nm),[81] below which droplet curvature effects are important.

In the region of interest in the microfluidic device, a movie records droplets traveling into the contracting region at high frame rates (usually about 20 000 frames per second) and captures droplet location and shape as it travels through the channel. Movies are typically less than one second in real time and contain ~100 to 1000 individual droplets. Each frame of the movie is analyzed to determine droplet location (center of mass) and principal radii for all droplets in the frame. Analyzing each frame successively to follow individual droplets across the device determines droplet velocity and the change of these derived variables with location.

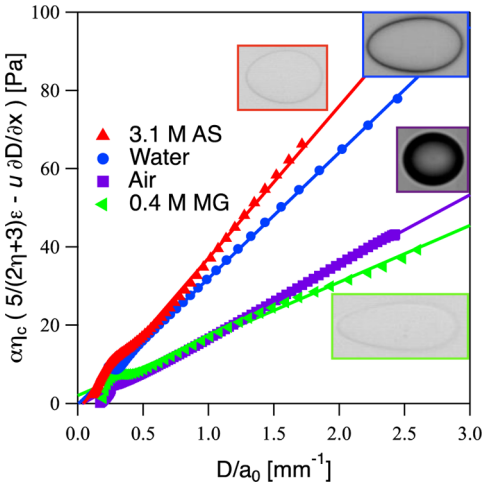

Figure 1. Taylor plot (from eq 7) for four individual droplets (3.1 M ammonium sulfate (AS), 0.4 M methylglyoxal (MG), and water) or bubble (air) in silicone oil. Each symbol is from a single frame of a movie tracking the individual droplets traveling through the microfluidic device. The solid lines are linear regressions to the data for each individual droplet, as described in the text. Bright-field raw images (not to scale) of the deformed droplets and bubble (equivalent diameters ~40—105 μm) are shown to demonstrate the level of phase contrast for each type of dispersed phase.

The analysis follows previous work[73,77] with modifications in the mathematical treatment when poor phase contrast (e.g., see the images for 3.1 M AS and 0.4 M MG droplets in Figure 1) causes noise in the retrieved variables. After deformation and velocity are determined for a droplet's entire travel across the image, from the wide region of low extensional shear to the converging region of larger extensional shear, a polynomial of order 7 is fit to both $D(x)$ and $u(x)$ for all points where $D(x) <$ 0.1 along the droplet's path. Derivatives of these polynomial fits yield $\frac{\partial D(x)}{\partial x}$ and $\dot{\varepsilon} = \frac{\partial u(x)}{\partial x}$ in eq 7. Interfacial tension is found by plotting the left-hand side of eq 7 versus $D(x)/a_0$, as shown in Figure 1. On this "Taylor plot,"[73] a line is fit over moderate deformations of $0.3 \leq D(x)/a_0 \leq 2$, following criteria by Cabral and Hudson (2006).[77] The trend of the raw data at $D(x)/a_0 \leq$ 0.3 is dominated by the shapes of the polynomial fits and their derivatives at the edges of the limits used in the fit and thus do not represent physical phenomena in the drop deformation dynamics. The slope of the linear regression yields interfacial tension, γ, for each individual droplet, and there is negligible change in the linear fit whether it is forced through the origin or not. The range of deformation from 0.3 to 2 is large enough to be above any small oscillations in $D(x)$ and $u(x)$ values in eq 7 but small enough to avoid droplet rupture and breakup events. Note that despite the use of polynomial fits to smooth out noise, the final linear fit to the data is still susceptible to considerable variance when the image contrast is low. A sensitivity analysis reveals that the retrieved IFT is more sensitive to the droplet radii than to viscosity. For an uncertainty in the major or minor radii of 1%, which for these experiments is ~2 pixels, the IFT can vary by as much as 15%. Fortunately, due to the large number of measurements performed in a single experiment, the median IFT value does not change significantly, although the variance (error) for that median IFT value will increase as the radii uncertainty increases. Viscosity, however, has very little effect on the retrieved IFT. Even moderate uncertainties in viscosity of

DOI: 10.1021/acs.est.5b04880
Environ. Sci. Technol. 2016, 50, 1251−1259

~30% yield a change in IFT of < ~0.1%. For a single experimental interfacial tension value, hundreds of individual droplets are analyzed. The distribution of single-droplet values are then compiled and a Gaussian function is fit to a histogram (see inset, Figure 2) of these values to yield the median interfacial tension with statistical uncertainty (the standard deviation of the Gaussian peak). A broader distribution of single-droplet values is typically observed for those samples with poor phase contrast or with few sample drops.

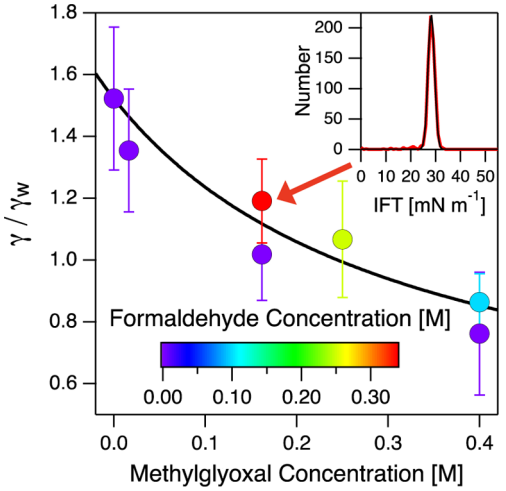

Figure 2. Relative interfacial tension at a reaction time of ~24 h as a function of initial methylglyoxal (MG) content in 3.1 M ammonium sulfate (AS) solutions. The interfacial tension (IFT) is reported relative to that of water−silicone oil, γ_w. Marker colors indicate the amount of formaldehyde (F) in the solution. Error bars indicate statistical uncertainty of each measurement sample, given as the variance of the Gaussian probability distribution (inset) of measurements for hundreds of individual droplets at each concentration and time. The solid line is a Langmuir-like curve (eq 8) fit to the data, with parameters γ_0 = 1.52, S = 1.21, and b = 3.13. The inset graph shows a histogram (red) of droplet IFT values with a Gaussian fit (black), the median and variance of which is used to plot the experimental IFT for the solution of 0.162 M MG−0.338 M F−3.1 M AS (indicated with an arrow).

Details of the microfluidic device fabrication are as follows. From the device design criteria[73] mentioned earlier, a photolithography mask is drawn in DraftSight (Dassault Systèmes) and printed on a 20 000 dpi high-resolution printer (CAD/Art Services, Inc.). A mold is prepared from this mask in a clean-room facility using standard photolithography techniques,[82−87] producing a silicon wafer that becomes a reusable master mold upon which the microfluidic devices are made. The microfluidic devices are constructed out of poly(dimethylsiloxane) (PDMS, Sylgard 184 Silicone Elastomer, Dow Corning Corporation), chosen for its ease in rapid prototyping[88] and successful applications in the microfluidic community.[73,79,84−86,89−96] PDMS is cured over the master mold, and individual devices are cut from the wafer and sealed to a glass microscope slide coverslip. The microfluidic experiments are performed on an Olympus IX73 inverted microscope with phase contrast and bright-field imaging. Pressure-driven flow is generated by syringe pumps (Harvard Apparatus) with gas-tight syringes connected to PFA tubing and needles hermetically sealed to the PDMS device. Imaging is done with a Photron FASTCAM Mini UX100 high-speed camera.

To properly quantify IFT, we independently measured the shear viscosity of the studied systems as a function of reaction time on an AR-G2 Rheometer from TA Instruments using a cup and bob geometry. A Mettler Toledo SevenExcellence multiparameter pH/conductivity meter was used to measure pH. Bulk-phase IFT measurements were performed on a Krüss Advanced Drop Shape Analysis Tensiometer using the pendant-drop method. Using this method, we measured the IFT between water and silicone oil to be 24.27 ± 0.73 mN m^{-1}, compared to 25.04 ± 2.31 mN m^{-1} with the microfluidic method. We also measured the IFT between 0.31 M ammonium sulfate solution and silicone oil to be 26.57 ± 2.32 mN m^{-1}, compared to 25.46 ± 1.98 mN m^{-1} with the microfluidic method. These measurements are in agreement with prior validations of the microfluidic tensiometer method.[73]

In all experiments, the continuous-phase fluid is silicone oil (poly(dimethylsiloxane), Fisher Scientific, CAS 63148-62-9). In general, silicone oils consist of a linear chain of siloxane repeating units with various radical side groups,[97] resulting in a hydrophobic oil with a potentially high viscosity. In this study, silicone oil is used as a proxy for an immiscible organic phase that might be found attached to an aqueous phase in atmospheric aerosol. We measured a viscosity of 45.08 ± 0.63 mPa s and a surface tension of 18.11 ± 1.28 mN m^{-1} for the specific silicone oil used here.

The dispersed phase fluid contains the solutions of interest. All water used in this study is HPLC-grade water (Sigma-Aldrich, CAS 7732−18−8). Stock solutions containing 3.1 M ammonium sulfate (AS, Avantor Performance Materials, CAS 7783−20−2) in HPLC water are mixed and used to make the organic solutions. Aqueous solutions up to 3.1 M AS are used to mimic ambient aerosol salt content.[64,98−101] Methylglyoxal solutions are prepared by adding the prescribed volume of a 40 wt % aqueous MG stock solution (Sigma-Aldrich, CAS 78-98-8) to the AS solutions. Solutions containing formaldehyde were added from a 37 wt % aqueous F stock solution (Sigma-Aldrich, CAS 50-00-0). All dispersed phase solutions in this study were stored in Pyrex jars with no special treatment to shield the jars from visible light, similar to previous studies.[64,102] Results will be discussed in terms of reaction time, which is the time passed since adding the organic(s) to 3.1 M AS solution.

RESULTS AND DISCUSSION

Previous work has established that the addition of methylglyoxal to aqueous ammonium sulfate significantly suppresses the *surface* (aqueous−air) tension of the mixture.[64] Figure 2 shows normalized *interfacial* (aqueous−oil) tension as a function of MG content in 3.1 M AS solution, showing a similar trend as that of surface tension (cf. Figure 4, Sareen et al., 2010).[64] At low MG content, relative IFT is greater than 1 owing to the higher IFT for 3.1 M AS solution (38.13 ± 4.60 mN m^{-1}) than for water (25.04 ± 2.31 mN m^{-1}). As MG is increased, IFT decreases and approaches a minimum value. The dependence of IFT on MG content can be fit with a Langmuir-like curve,[64,103]

$$\gamma = \gamma_0 - S\frac{bM_0}{1 + bM_0} \tag{8}$$

where γ_0 is the IFT with no MG, M_0 is the MG concentration, and S and b are fit parameters. For the fit shown in Figure 2, γ_0,

DOI: 10.1021/acs.est.5b04880
Environ. Sci. Technol. 2016, 50, 1251−1259

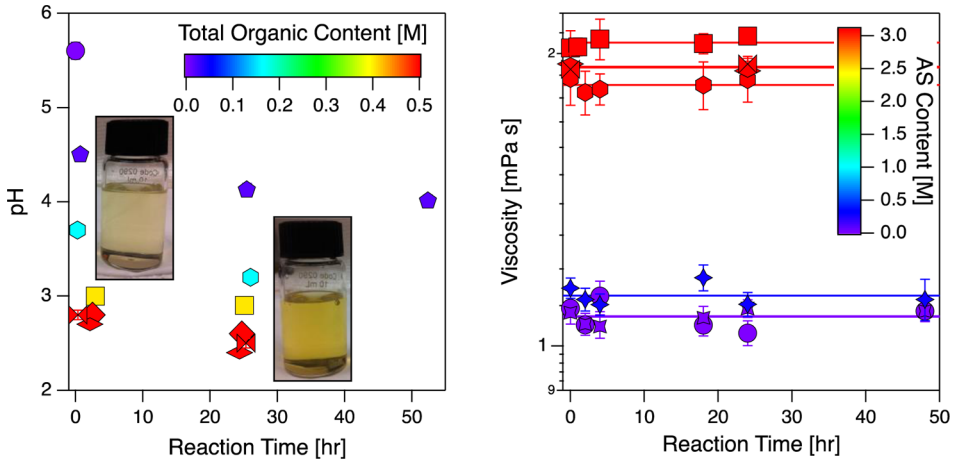

Figure 3. Solution pH (left) and viscosity (right) as a function of reaction time. Markers are colored by total organic content (left) and ammonium sulfate (AS) content (right) spanning the range of values used in this study. Error bars are one standard deviation; note that the error bars on the pH data are small enough to be hidden by the markers. Solid lines (right) are the average viscosities for each system. The images are vials of 0.162 M methylglyoxal in 3.1 M ammonium sulfate just after mixing (left) and after 24 h of reacting time (right).

S, b = 1.52, 1.21, and 3.13, respectively. Over the range of MG concentration used, the trends of IFT suppression are the same as those previously reported for surface tension of this chemical system.

The IFT results in Figure 2 are measurements taken ~24 h after the addition of the organic(s) to the AS solution. Over this reaction time, solutions containing MG become progressively darker (see pictures in Figure 3) due to the formation of light-absorbing compounds in solution, resulting in a change in solution alkalinity (Figure 3, left). Recall that the fluid properties in eq 7 include solution viscosity as well as interfacial tension, so a change with time of the deformation behavior of the droplet could be due to a change in viscosity as the solution ages. However, within measurement uncertainty, the viscosity of the aqueous solutions containing varying amounts of MG and AS does not change with reaction time (Figure 3, right). Because the bulk solution viscosity is constant in time, any differences in behavior of the droplet are explained through differences in the interfacial properties alone.

Previously, the surface tension of ternary mixtures of MG and F in 3.1 M AS solution have been shown to largely follow (within ~10%) a single-component Szyszkowski–Langmuir curve.[71,72] Although the more-comprehensive Henning model[104] has been shown to describe well the behavior of surface tension for both nonreactive[104] and reactive[99] mixtures of organics, when accounting for the formaldehyde component in the Henning model, there is a larger deviation between measured and modeled values of surface tension.[71,72] These results indicate that for a MG–F–AS system, surface tension is largely governed by the amount of MG. As one might expect, the interfacial behavior of the same system here (Figure 2) behaves likewise, where the interfacial tension suppression is driven by MG, not F, content.

Results for interfacial tension measurements as a function of age are shown in Figure 4. Previous results for surface tension have indicated that after addition of MG to aqueous AS solutions, the measured surface tension will decrease over ~24 h to a minimum value.[64] In contrast, it was found that IFT remained largely constant with reaction time for the MG—AS systems (Figure 4, top). MG has been shown to adsorb very slowly to the air–water interface in aqueous solutions;[65] thus, the rapid equilibration of IFT to oil could be the result of the

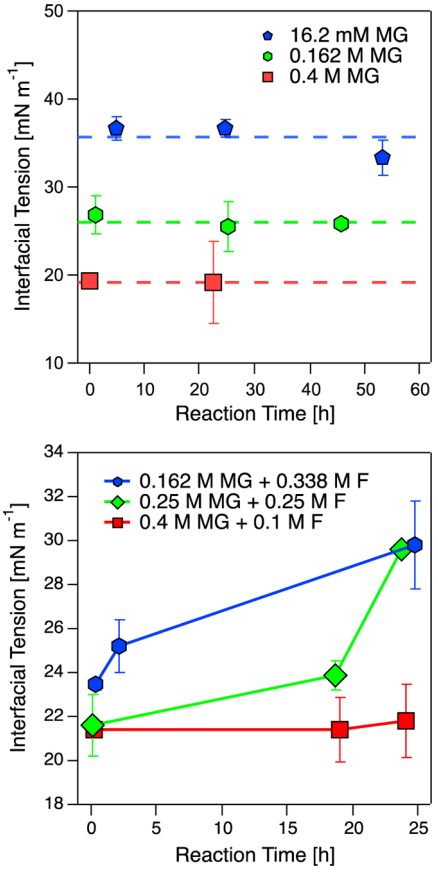

Figure 4. Interfacial tension as a function of reaction time for methylglyoxal (MG)–ammonium sulfate (AS) systems (top) and methylglyoxal–formaldehyde–ammonium sulfate systems (bottom). All solutions are in 3.1 M AS. Dashed lines (top) indicate average values for each system over all measurement times. Solid lines (bottom) connect the data points within each system as a guideline and do not indicate any functional dependence. Each data series is from a single solution allowed to react over the time displayed. Error bars on all data points show statistical uncertainty in the measurements.

DOI: 10.1021/acs.est.5b04880
Environ. Sci. Technol. 2016, 50, 1251–1259

microfluidic technique using a much smaller volume of solution than traditional bulk methods, where dissolved species need to travel far to find the interface. Even in pendant-drop experiments that can approach a similar droplet volume (~2−16 mm^3)[105] to those in this microfluidic study (~3−200 × 10^{-5} mm^3), suggesting that equilibration time may be similar, the pendant-drop method is such that the droplet essentially has an infinite reservoir of surfactant available to the droplet interface, whereas the microfluidic droplets do not.

To infer ambient aerosol morphology from these results, one can use the measured IFT values in eq 3 in combination with surface tensions previously reported.[64] For the MG−AS systems studied here, complete engulfing ($S_2 > 0$, $S_3 < 0$) is predicted for all concentrations of MG, and the change in surface tension with reaction time reported by Sareen et al. (2010)[64] is not a large enough change to cause a change in sign of either S_2 or S_3.

Surprisingly, in the presence of formaldehyde, aging effects on interfacial tension become apparent (Figure 4, bottom). At the largest amount of MG content, the IFT remained constant with reaction time, behaving largely like the system with 0.4 M MG in 3.1 M AS displayed in the top of Figure 4. As the MG content decreases and F content increases, the IFT of the fresh mixture increases, and the change in IFT with age becomes more pronounced. For all three MG−F systems, the total organic content was fixed at 0.5 M and IFT suppression at ~24 h reaction time for these systems is consistent with MG-only systems of similar MG content (Figure 2). The F dependence is a notable difference in these systems' IFT behavior with oil versus surface tension with air. Clearly, there is additional complexity to the chemical aging of these systems that is causing the surface activity to change with reaction time. To elucidate these differences, a future study on the detailed time-dependent chemistry of this system should be performed, specifically to look for the behavior of surface-active species. As has been established for MG systems, the singly hydrated MG is a likely candidate as an important surface-active species.[65] Although this compound was observed in MG−F−AS systems,[71] it is unclear if this product might be consumed in later generations of reaction products, leading to an overall decrease in surface activity of the mixture.

The increase in IFT with chemical age for this system is consistent with an overall trend that lower-volatility oxidized (aged) organic aerosol shows a smaller departure from the surface tension of water than more hydrocarbon-like (fresh) organic aerosol (cf. Figure 6, McNeill et al., 2014).[7] Returning to eq 3 to infer ambient aerosol morphology of these systems, once again, complete engulfing is initially predicted for all ternary MG−F−AS systems studied here. However, in contrast to the binary MG−AS system, the large change in IFT with reaction time for the 0.25 M MG−0.25 M MG F system is large enough for S_2 to trend from a positive to negative value (within statistical uncertainty), meaning that this system is trending from complete engulfing toward a partial engulfing morphology.

This study has demonstrated the first use of a microfluidic experimental platform to investigate the interfacial properties of atmospheric aerosol mimics to assess the surface activity of dissolved constituents. In the current configuration, this platform allows rapid, repeatable measurements of interfacial tension between two immiscible liquids in a parameter space inaccessible to bulk measurements due to lengthy equilibration time scales of either the interface or the measurement itself. The results show that the interfacial tension of aqueous ammonium sulfate−methylglyoxal solutions to silicone oil have an interfacial tension depression similar to that of the solutions' surface tension depression.[64] However, unlike previous results for surface (aqueous−air) tension, the behavior of interfacial (aqueous−oil) tension of these solutions with the addition of formaldehyde exhibits a dependence on reaction time, indicating additional complexities as a result of species competition within the solution. Future work will assess a possible explanation for these complexities by considering the effect that depletion[78] might have on these chemical systems at the scale of atmospheric aerosol, by exploring alternate continuous phases for use in droplet microfluidic devices, and by performing bubble microfluidic tensiometry (for aqueous−air measurements).

AUTHOR INFORMATION

Corresponding Author

*Phone: 612-624-0428; e-mail: cdutcher@umn.edu.

Notes

The authors declare no competing financial interest.

ACKNOWLEDGMENTS

We gratefully acknowledge Prof. Gordon Christopher for sharing device design files to aid in the startup of this project and Prof. Kevin Dorfman for allowing use of his laboratory and equipment for fabrication of the PDMS microfluidic devices. We also thank Christopher Nelson, Drs. Zhicheng Long and Rebecca Dylla-Spears, and Profs. Shelley Anna and Lynn Walker for useful discussions. Part of this work was carried out in the College of Science and Engineering Minnesota Nano Center, University of Minnesota, which receives partial support from NSF through the NNIN program. Part of this work was carried out in the College of Science and Engineering Coating Process and Visualization Laboratory and the Polymer Characterization Facility, University of Minnesota, which have received capital equipment funding from the NSF through the UMN MRSEC under award DMR-1420013. H.C.B. was supported through a National Science Foundation Graduate Research Fellowship. C.S.D. was partially supported by a 3M Nontenured Faculty Award. This material is based upon work supported by the National Science Foundation under grant no. AGS-1433514.

ABBREVIATIONS

SOA	secondary organic aerosol
MG	methylglyoxal
AS	ammonium sulfate
F	formaldehyde
IFT	interfacial tension

REFERENCES

(1) Seinfeld, J. H.; Pandis, S. N. *Atmospheric Chemistry and Physics: From Air Pollution to Climate Change*, 2nd ed.; John Wiley & Sons, Inc.: New York, 2006; 1−1233.

(2) Zhang, Q.; Jimenez, J. L.; Canagaratna, M. R.; Allan, J. D.; Coe, H.; Ulbrich, I.; Alfarra, M. R.; Takami, A.; Middlebrook, A. M.; Sun, Y. L.; et al. Ubiquity and dominance of oxygenated species in organic aerosols in anthropogenically-influenced Northern Hemisphere midlatitudes. *Geophys. Res. Lett.* **2007**, *34* (13), L13801.

(3) Jimenez, J. L.; Canagaratna, M. R.; Donahue, N. M.; Prévôt, A. S. H.; Zhang, Q.; Kroll, J. H.; DeCarlo, P. F.; Allan, J. D.; Coe, H.; Ng, N.

DOI: 10.1021/acs.est.5b04880
Environ. Sci. Technol. 2016, 50, 1251−1259

L.; et al. Evolution of organic aerosols in the atmosphere. *Science* **2009**, *326* (5959), 1525−1529.
(4) Hallquist, M.; Wenger, J. C.; Baltensperger, U.; Rudich, Y.; Simpson, D.; Claeys, M.; Dommen, J.; Donahue, N. M.; George, C.; Goldstein, A. H.; et al. The formation, properties and impact of secondary organic aerosol: Current and emerging issues. *Atmos. Chem. Phys.* **2009**, *9* (14), 5155−5236.
(5) Goldstein, A. H.; Galbally, I. E. Known and unexplored organic constituents in the earth's atmosphere. *Environ. Sci. Technol.* **2007**, *41* (5), 1514−1521.
(6) McNeill, V. F. Aqueous organic chemistry in the atmosphere: Sources and chemical processing of organic aerosols. *Environ. Sci. Technol.* **2015**, *49* (3), 1237−1244.
(7) McNeill, V. F.; Sareen, N.; Schwier, A. N. Surface-active organics in atmospheric aerosols. *Top. Curr. Chem.* **2013**, *339*, 201−259.
(8) Facchini, M. C.; Decesari, S.; Mircea, M.; Fuzzi, S.; Loglio, G. Surface tension of atmospheric wet aerosol and cloud/fog droplets in relation to their organic carbon content and chemical composition. *Atmos. Environ.* **2000**, *34* (28), 4853−4857.
(9) Taraniuk, I.; Graber, E. R.; Kostinski, A.; Rudich, Y. Surfactant properties of atmospheric and model humic-like substances (HULIS). *Geophys. Res. Lett.* **2007**, *34* (16), L16807.
(10) Zuend, A.; Marcolli, C.; Peter, T.; Seinfeld, J. H. Computation of liquid-liquid equilibria and phase stabilities: Implications for RH-dependent gas/particle partitioning of organic-inorganic aerosols. *Atmos. Chem. Phys.* **2010**, *10* (16), 7795−7820.
(11) McNeill, V. F.; Patterson, J.; Wolfe, G. M.; Thornton, J. A. The effect of varying levels of surfactant on the reactive uptake of N_2O_5 to aqueous aerosol. *Atmos. Chem. Phys.* **2006**, *6* (6), 1635−1644.
(12) Folkers, M.; Mentel, T. F.; Wahner, A. Influence of an organic coating on the reactivity of aqueous aerosols probed by the heterogeneous hydrolysis of N_2O_5. *Geophys. Res. Lett.* **2003**, *30* (12), 1644.
(13) Shulman, M. L.; Charlson, R. J.; James Davis, E. The effects of atmospheric organics on aqueous droplet evaporation. *J. Aerosol Sci.* **1997**, *28* (5), 737−752.
(14) Buajarern, J.; Mitchem, L.; Reid, J. P. Characterizing the formation of organic layers on the surface of inorganic/aqueous aerosols by Raman spectroscopy. *J. Phys. Chem. A* **2007**, *111* (46), 11852−11859.
(15) Davies, J. F.; Miles, R. E. H.; Haddrell, A. E.; Reid, J. P. Influence of organic films on the evaporation and condensation of water in aerosol. *Proc. Natl. Acad. Sci. U. S. A.* **2013**, *110* (22), 8807−8812.
(16) Baustian, K. J.; Cziczo, D. J.; Wise, M. E.; Pratt, K. A.; Kulkarni, G.; Hallar, A. G.; Tolbert, M. A. Importance of aerosol composition, mixing state, and morphology for heterogeneous ice nucleation: A combined field and laboratory approach. *J. Geophys. Res.* **2012**, *117* (D6), D06217.
(17) Lance, S.; Nenes, A.; Rissman, T. A. Chemical and dynamical effects on cloud droplet number: Implications for estimates of the aerosol indirect effect. *J. Geophys. Res.* **2004**, *109* (D22), D22208.
(18) Ellison, G. B.; Tuck, A. F.; Vaida, V. Atmospheric processing of organic aerosols. *J. Geophys. Res.* **1999**, *104* (D9), 11633−11641.
(19) Bertram, A. K.; Ivanov, A. V.; Hunter, M.; Molina, L. T.; Molina, M. J. The reaction probability of OH on organic surfaces of tropospheric interest. *J. Phys. Chem. A* **2001**, *105* (41), 9415−9421.
(20) George, I. J.; Abbatt, J. P. D. Heterogeneous oxidation of atmospheric aerosol particles by gas-phase radicals. *Nat. Chem.* **2010**, *2* (9), 713−722.
(21) Lang-Yona, N.; Abo-Riziq, A.; Erlick, C.; Segre, E.; Trainic, M.; Rudich, Y. Interaction of internally mixed aerosols with light. *Phys. Chem. Chem. Phys.* **2010**, *12* (1), 21−31.
(22) Wise, M. E.; Baustian, K. J.; Tolbert, M. A. Internally mixed sulfate and organic particles as potential ice nuclei in the tropical tropopause region. *Proc. Natl. Acad. Sci. U. S. A.* **2010**, *107* (15), 6693−6698.
(23) Garland, R. M.; Wise, M. E.; Beaver, M. R.; DeWitt, H. L.; Aiken, A. C.; Jimenez, J. L.; Tolbert, M. A. Impact of palmitic acid coating on the water uptake and loss of ammonium sulfate particles. *Atmos. Chem. Phys.* **2005**, *5* (7), 1951−1961.
(24) Chan, M.; Chan, C. K. Mass transfer effects on the hygroscopic growth of ammonium sulfate particles with a water-insoluble coating. *Atmos. Environ.* **2007**, *41* (21), 4423−4433.
(25) Wise, M. E.; Garland, R. M.; Tolbert, M. A. Ice nucleation in internally mixed ammonium sulfate/dicarboxylic acid particles. *J. Geophys. Res.* **2004**, *109* (D19), D19203.
(26) Pankow, J. F. An absorption model of the gas/aerosol partitioning involved in the formation of secondary organic aerosol. *Atmos. Environ.* **1994**, *28* (2), 189−193.
(27) O'Brien, R. E.; Wang, B.; Kelly, S. T.; Lundt, N.; You, Y.; Bertram, A. K.; Leone, S. R.; Laskin, A.; Gilles, M. K. Liquid−liquid phase separation in aerosol particles: Imaging at the nanometer scale. *Environ. Sci. Technol.* **2015**, *49* (8), 4995−5002.
(28) You, Y.; Renbaum-Wolff, L.; Carreras-Sospedra, M.; Hanna, S. J.; Hiranuma, N.; Kamal, S.; Smith, M. L.; Zhang, X.; Weber, R. J.; Shilling, J. E.; et al. Images reveal that atmospheric particles can undergo liquid−liquid phase separations. *Proc. Natl. Acad. Sci. U. S. A.* **2012**, *109* (33), 13188−13193.
(29) Kwamena, N. O. A.; Buajarern, J.; Reid, J. P. Equilibrium morphology of mixed organic/inorganic/aqueous aerosol droplets: Investigating the effect of relative humidity and surfactants. *J. Phys. Chem. A* **2010**, *114* (18), 5787−5795.
(30) Gill, P. S.; Graedel, T. E.; Weschler, C. J. Organic films on atmospheric aerosol particles, fog droplets, cloud droplets, raindrops, and snowflakes. *Rev. Geophys.* **1983**, *21* (4), 903−920.
(31) Freedman, M. A.; Baustian, K. J.; Wise, M. E.; Tolbert, M. A. Characterizing the morphology of organic aerosols at ambient temperature and pressure. *Anal. Chem.* **2010**, *82* (19), 7965−7972.
(32) Bertram, A. K.; Martin, S. T.; Hanna, S. J.; Smith, M. L.; Bodsworth, A.; Chen, Q.; Kuwata, M.; Liu, A.; You, Y.; Zorn, S. R. Predicting the relative humidities of liquid-liquid phase separation, efflorescence, and deliquescence of mixed particles of ammonium sulfate, organic material, and water using the organic-to-sulfate mass ratio of the particle and the oxygen-to-carbon elemental ratio of the organic component. *Atmos. Chem. Phys.* **2011**, *11* (21), 10995−11006.
(33) Song, M.; Marcolli, C.; Krieger, U. K.; Lienhard, D. M.; Peter, T. Morphologies of mixed organic/inorganic/aqueous aerosol droplets. *Faraday Discuss.* **2013**, *165*, 289−316.
(34) Reid, J. P.; Dennis-Smither, B. J.; Kwamena, N.-O. A.; Miles, R. E. H.; Hanford, K. L.; Homer, C. J. The morphology of aerosol particles consisting of hydrophobic and hydrophilic phases: hydrocarbons, alcohols and fatty acids as the hydrophobic component. *Phys. Chem. Chem. Phys.* **2011**, *13* (34), 15559.
(35) Buajarern, J.; Mitchem, L.; Reid, J. P. Characterizing multiphase organic/inorganic/aqueous aerosol droplets. *J. Phys. Chem. A* **2007**, *111* (37), 9054−9061.
(36) Assovskii, I. G.; Rashkovskii, S. A. Relaxation of drops of a mixture of two immiscible liquids to equilibrium shapes. *Dokl. Phys. Chem.* **2002**, *385* (1−3), 149−153.
(37) Tabazadeh, A. Organic aggregate formation in aerosols and its impact on the physicochemical properties of atmospheric particles. *Atmos. Environ.* **2005**, *39* (30), 5472−5480.
(38) Freney, E. J.; Adachi, K.; Buseck, P. R. Internally mixed atmospheric aerosol particles: Hygroscopic growth and light scattering. *J. Geophys. Res.* **2010**, *115* (D19), D19210.
(39) Ciobanu, V. G.; Marcolli, C.; Krieger, U. K.; Weers, U.; Peter, T. Liquid−liquid phase separation in mixed organic/inorganic aerosol particles. *J. Phys. Chem. A* **2009**, *113* (41), 10966−10978.
(40) Song, M.; Marcolli, C.; Krieger, U. K.; Zuend, A.; Peter, T. Liquid-liquid phase separation and morphology of internally mixed dicarboxylic acids/ammonium sulfate/water particles. *Atmos. Chem. Phys.* **2012**, *12* (5), 2691−2712.
(41) Cistola, D. P.; Hamilton, J. A.; Jackson, D.; Small, D. M. Ionization and phase behavior of fatty acids in water: Application of the Gibbs phase rule. *Biochemistry* **1988**, *27* (6), 1881−1888.

DOI: 10.1021/acs.est.5b04880
Environ. Sci. Technol. 2016, 50, 1251−1259

(42) Maria, S. F.; Russell, L. M.; Gilles, M. K.; Myneni, S. C. B. Organic aerosol growth mechanisms and their climate-forcing implications. *Science* **2004**, *306* (5703), 1921−1924.
(43) Torza, S.; Mason, S. G. Three-phase interactions in shear and electrical fields. *J. Colloid Interface Sci.* **1970**, *33* (1), 67−83.
(44) Harkins, W. D.; Feldman, A. Films. The Spreading of Liquids and the Spreading Coefficient. *J. Am. Chem. Soc.* **1922**, *44* (12), 2665−2685.
(45) Harkins, W. D. *The Physical Chemistry of Surface Films*; Reinhold Publishing Corporation: New York, 1952.
(46) Shaw, D. J. *Introduction to Colloid and Surface Chemistry*, 4th ed.; Butterworth-Heinemann Ltd: London, 1992.
(47) de Gennes, P.-G.; Brochard-Wyart, F.; Quéré, D. *Capillarity and Wetting Phenomena*; Springer Science & Business Media: New York, 2004.
(48) Qiu, Y.; Molinero, V. Morphology of liquid−liquid phase separated aerosols. *J. Am. Chem. Soc.* **2015**, *137* (33), 10642−10651.
(49) Grosjean, D.; Williams, E. L., II; Grosjean, E. Atmospheric chemistry of isoprene and of its carbonyl products. *Environ. Sci. Technol.* **1993**, *27* (5), 830−840.
(50) Tuazon, E. C.; Atkinson, R.; Mac Leod, H.; Biermann, H. W.; Winer, A. M.; Carter, W. P. L.; Pitts, J. N., Jr. Yields of glyoxal and methylglyoxal from the NO_X-air photooxidations of toluene and *m*- and *p*-xylene. *Environ. Sci. Technol.* **1984**, *18* (12), 981−984.
(51) Tuazon, E. C.; MacLeod, H.; Atkinson, R.; Carter, W. P. L. α-Dicarbonyl yields from the NO_X-air photooxidations of a series of aromatic hydrocarbons in air. *Environ. Sci. Technol.* **1986**, *20* (4), 383−387.
(52) Smith, D. F.; Kleindienst, T. E.; McIver, C. D. Primary product distributions from the reaction of OH with *m*-, *p*-xylene, 1,2,4- and 1,3,5-trimethylbenzene. *J. Atmos. Chem.* **1999**, *34* (3), 339−364.
(53) Paulsen, D.; Dommen, J.; Kalberer, M.; Prévôt, A. S. H.; Richter, R.; Sax, M.; Steinbacher, M.; Weingartner, E.; Baltensperger, U. Secondary organic aerosol formation by irradiation of 1,3,5-trimethylbenzene−NO_X−H_2O in a new reaction chamber for atmospheric chemistry and physics. *Environ. Sci. Technol.* **2005**, *39* (8), 2668−2678.
(54) Zhao, J.; Zhang, R.; Misawa, K.; Shibuya, K. Experimental product study of the OH-initiated oxidation of m-xylene. *J. Photochem. Photobiol., A* **2005**, *176* (1−3), 199−207.
(55) Grosjean, E.; Grosjean, D.; Fraser, M. P.; Cass, G. R. Air quality model evaluation data for organics. 2. C_1−C_{14} carbonyls in Los Angeles air. *Environ. Sci. Technol.* **1996**, *30* (9), 2687−2703.
(56) Grosjean, D.; Grosjean, E.; Moreira, L. F. R. Speciated ambient carbonyls in Rio de Janeiro, Brazil. *Environ. Sci. Technol.* **2002**, *36* (7), 1389−1395.
(57) Fraser, M. P.; Kleeman, M. J.; Schauer, J. J.; Cass, G. R. Modeling the atmospheric concentrations of individual gas-phase and particle-phase organic compounds. *Environ. Sci. Technol.* **2000**, *34* (7), 1302−1312.
(58) Sareen, N.; Schwier, A. N.; Lathem, T. L.; Nenes, A.; McNeill, V. F. Surfactants from the gas phase may promote cloud droplet formation. *Proc. Natl. Acad. Sci. U. S. A.* **2013**, *110* (8), 2723−2728.
(59) Loeffler, K. W.; Koehler, C. A.; Paul, N. M.; De Haan, D. O. Oligomer formation in evaporating aqueous glyoxal and methyl glyoxal solutions. *Environ. Sci. Technol.* **2006**, *40* (20), 6318−6323.
(60) Zhao, J.; Levitt, N. P.; Zhang, R.; Chen, J. Heterogeneous reactions of methylglyoxal in acidic media: Implications for secondary organic aerosol formation. *Environ. Sci. Technol.* **2006**, *40* (24), 7682−7687.
(61) Barsanti, K. C.; Pankow, J. F. Thermodynamics of the formation of atmospheric organic particulate matter by accretion reactions—2. Dialdehydes, methylglyoxal, and diketones. *Atmos. Environ.* **2005**, *39* (35), 6597−6607.
(62) Sempéré, R.; Kawamura, K. Comparative distributions of dicarboxylic acids and related polar compounds in snow, rain and aerosols from urban atmosphere. *Atmos. Environ.* **1994**, *28* (3), 449−459.
(63) Blando, J. D.; Turpin, B. J. Secondary organic aerosol formation in cloud and fog droplets: a literature evaluation of plausibility. *Atmos. Environ.* **2000**, *34* (10), 1623−1632.
(64) Sareen, N.; Schwier, A. N.; Shapiro, E. L.; Mitroo, D.; McNeill, V. F. Secondary organic material formed by methylglyoxal in aqueous aerosol mimics. *Atmos. Chem. Phys.* **2010**, *10* (3), 997−1016.
(65) Wren, S. N.; Gordon, B. P.; Valley, N. A.; McWilliams, L. E.; Richmond, G. L. Hydration, orientation, and conformation of methylglyoxal at the air−water interface. *J. Phys. Chem. A* **2015**, *119* (24), 6391−6403.
(66) Grutter, M.; Flores, E.; Andraca-Ayala, G.; Báez, A. Formaldehyde levels in downtown Mexico City during 2003. *Atmos. Environ.* **2005**, *39* (6), 1027−1034.
(67) Finlayson-Pitts, B. J.; Pitts, J. N., Jr. *Chemistry of the Upper and Lower Atmosphere: Theory, Experiments, and Applications*; Elsevier Science: Amsterdam, The Netherlands, 2000.
(68) Wang, X.; Gao, S.; Yang, X.; Chen, H.; Chen, J.; Zhuang, G.; Surratt, J. D.; Chan, M.; Seinfeld, J. H. Evidence for high molecular weight nitrogen-containing organic salts in urban aerosols. *Environ. Sci. Technol.* **2010**, *44* (12), 4441−4446.
(69) Balashov, A. L.; Krasnov, V. L.; Danov, S. M.; Chernov, A. Y.; Sulimov, A. V. Formation of cyclic oligomers in concentrated aqueous solutions of formaldehyde. *J. Struct. Chem.* **2001**, *42* (3), 398−403.
(70) Toda, K.; Yunoki, S.; Yanaga, A.; Takeuchi, M.; Ohira, S.-I.; Dasgupta, P. K. Formaldehyde content of atmospheric aerosol. *Environ. Sci. Technol.* **2014**, *48* (12), 6636−6643.
(71) Li, Z.; Schwier, A. N.; Sareen, N.; McNeill, V. F. Reactive processing of formaldehyde and acetaldehyde in aqueous aerosol mimics: Surface tension depression and secondary organic products. *Atmos. Chem. Phys.* **2011**, *11* (22), 11617−11629.
(72) Li, Z.; Schwier, A. N.; Sareen, N.; McNeill, V. F. Corrigendum to "Reactive processing of formaldehyde and acetaldehyde in aqueous aerosol mimics: Surface tension depression and secondary organic products" published in Atmos. Chem. Phys., 11, 11617−11629, 2011. *Atmos. Chem. Phys.* **2012**, *12* (24), 11885−11887.
(73) Hudson, S. D.; Cabral, J. T.; Goodrum, W. J., Jr.; Beers, K. L.; Amis, E. J. Microfluidic interfacial tensiometry. *Appl. Phys. Lett.* **2005**, *87* (8), 081905.
(74) Taylor, G. I. The formation of emulsions in definable fields of flow. *Proc. R. Soc. London, Ser. A* **1934**, *146* (858), 501−523.
(75) Taylor, G. I. The viscosity of a fluid containing small drops of another fluid. *Proc. R. Soc. London, Ser. A* **1932**, *138* (834), 41−48.
(76) Rallison, J. M. The deformation of small viscous drops and bubbles in shear flows. *Annu. Rev. Fluid Mech.* **1984**, *16* (1), 45−66.
(77) Cabral, J. T.; Hudson, S. D. Microfluidic approach for rapid multicomponent interfacial tensiometry. *Lab Chip* **2006**, *6* (3), 427−436.
(78) Alvarez, N. J.; Walker, L. M.; Anna, S. L. A criterion to assess the impact of confined volumes on surfactant transport to liquid-fluid interfaces. *Soft Matter* **2012**, *8* (34), 8917−8925.
(79) Christopher, G. F.; Noharuddin, N. N.; Taylor, J. A.; Anna, S. L. Experimental observations of the squeezing-to-dripping transition in T-shaped microfluidic junctions. *Phys. Rev. E* **2008**, *78* (3), 036317.
(80) Anna, S. L.; Bontoux, N.; Stone, H. A. Formation of dispersions using "flow focusing" in microchannels. *Appl. Phys. Lett.* **2003**, *82* (3), 364.
(81) Bilde, M.; Barsanti, K.; Booth, M.; Cappa, C. D.; Donahue, N. M.; Emanuelsson, E. U.; McFiggans, G.; Krieger, U. K.; Marcolli, C.; Topping, D.; et al. Saturation vapor pressures and transition enthalpies of low-volatility organic molecules of atmospheric relevance: From dicarboxylic acids to complex mixtures. *Chem. Rev.* **2015**, *115* (10), 4115−4156.
(82) Duffy, D. C.; Schueller, O. J. A.; Brittain, S. T.; Whitesides, G. M. Rapid prototyping of microfluidic switches in poly(dimethyl siloxane) and their actuation by electro-osmotic flow. *J. Micromech. Microeng.* **1999**, *9* (3), 211−217.
(83) Effenhauser, C. S.; Bruin, G. J. M.; Paulus, A.; Ehrat, M. Integrated capillary electrophoresis on flexible silicone microdevices:

DOI: 10.1021/acs.est.5b04880
Environ. Sci. Technol. 2016, 50, 1251−1259

Analysis of DNA restriction fragments and detection of single DNA molecules on microchips. *Anal. Chem.* **1997**, *69* (17), 3451−3457.
(84) Schueller, O. J. A.; Duffy, D. C.; Rogers, J. A.; Brittain, S. T.; Whitesides, G. M. Reconfigurable diffraction gratings based on elastomeric microfluidic devices. *Sens. Actuators, A* **1999**, *78* (2−3), 149−159.
(85) Jackman, R. J.; Duffy, D. C.; Ostuni, E.; Willmore, N. D.; Whitesides, G. M. Fabricating large arrays of microwells with arbitrary dimensions and filling them using discontinuous dewetting. *Anal. Chem.* **1998**, *70* (11), 2280−2287.
(86) McDonald, J. C.; Duffy, D. C.; Anderson, J. R.; Chiu, D. T.; Wu, H.; Schueller, O. J. A.; Whitesides, G. M. Fabrication of microfluidic systems in poly(dimethylsiloxane). *Electrophoresis* **2000**, *21* (1), 27−40.
(87) Xia, Y.; Whitesides, G. M. Soft lithography. *Annu. Rev. Mater. Sci.* **1998**, *28* (1), 153−184.
(88) Duffy, D. C.; McDonald, J. C.; Schueller, O. J. A.; Whitesides, G. M. Rapid prototyping of microfluidic systems in poly-(dimethylsiloxane). *Anal. Chem.* **1998**, *70* (23), 4974−4984.
(89) Delamarche, E.; Bernard, A.; Schmid, H.; Michel, B.; Biebuyck, H. Patterned delivery of immunoglobulins to surfaces using microfluidic networks. *Science* **1997**, *276* (5313), 779−781.
(90) Delamarche, E.; Bernard, A.; Schmid, H.; Bietsch, A.; Michel, B.; Biebuyck, H. Microfluidic networks for chemical patterning of substrates: Design and application to bioassays. *J. Am. Chem. Soc.* **1998**, *120* (3), 500−508.
(91) Qin, D.; Xia, Y.; Whitesides, G. M. Rapid prototyping of complex structures with feature sizes larger than 20 μm. *Adv. Mater.* **1996**, *8* (11), 917−919.
(92) Tran, T. M.; Lan, F.; Thompson, C. S.; Abate, A. R. From tubes to drops: Droplet-based microfluidics for ultrahigh-throughput biology. *J. Phys. D: Appl. Phys.* **2013**, *46* (11), 114004.
(93) Seemann, R.; Brinkmann, M.; Pfohl, T.; Herminghaus, S. Droplet based microfluidics. *Rep. Prog. Phys.* **2012**, *75* (1), 016601.
(94) Tanyeri, M.; Ranka, M.; Sittipolkul, N.; Schroeder, C. M. A microfluidic-based hydrodynamic trap: Design and implementation. *Lab Chip* **2011**, *11* (10), 1786−1794.
(95) Tanyeri, M.; Schroeder, C. M. Manipulation and confinement of single particles using fluid flow. *Nano Lett.* **2013**, *13* (6), 2357−2364.
(96) Alvarez, N. J.; Walker, L. M.; Anna, S. L. A microtensiometer to probe the effect of radius of curvature on surfactant transport to a spherical interface. *Langmuir* **2010**, *26* (16), 13310−13319.
(97) Barca, F.; Caporossi, T.; Rizzo, S. Silicone oil: Different physical properties and clinical applications. *BioMed Res. Int.* **2014**, *2014* (5), 1−7.
(98) Shapiro, E. L.; Szprengiel, J.; Sareen, N.; Jen, C. N.; Giordano, M. R.; McNeill, V. F. Light-absorbing secondary organic material formed by glyoxal in aqueous aerosol mimics. *Atmos. Chem. Phys.* **2009**, *9* (7), 2289−2300.
(99) Schwier, A. N.; Sareen, N.; Mitroo, D.; Shapiro, E. L.; McNeill, V. F. Glyoxal-methylglyoxal cross-reactions in secondary organic aerosol formation. *Environ. Sci. Technol.* **2010**, *44* (16), 6174−6182.
(100) Tang, I. N.; Tridico, A. C.; Fung, K. H. Thermodynamic and optical properties of sea salt aerosols. *J. Geophys. Res.* **1997**, *102* (D19), 23269−23275.
(101) Tang, I. N.; Munkelwitz, H. R. Water activities, densities, and refractive indices of aqueous sulfates and sodium nitrate droplets of atmospheric importance. *J. Geophys. Res.* **1994**, *99* (D9), 18801−18808.
(102) Schwier, A. N.; Viglione, G. A.; Li, Z.; McNeill, V. F. Modeling the surface tension of complex, reactive organic-inorganic mixtures. *Atmos. Chem. Phys. Discuss.* **2013**, *13* (1), 549−580.
(103) Langmuir, I. The adsorption of gases on plane surfaces of glass, mica and platinum. *J. Am. Chem. Soc.* **1918**, *40* (9), 1361−1403.
(104) Henning, S.; Rosenørn, T.; D'Anna, B.; Gola, A. A.; Svenningsson, B.; Bilde, M. Cloud droplet activation and surface tension of mixtures of slightly soluble organics and inorganic salt. *Atmos. Chem. Phys.* **2005**, *5* (2), 575−582.
(105) Morita, A.; Carastan, D.; Demarquette, N. Influence of drop volume on surface tension evaluated using the pendant drop method. *Colloid Polym. Sci.* **2002**, *280* (9), 857−864.

DOI: 10.1021/acs.est.5b04880
Environ. Sci. Technol. 2016, 50, 1251−1259